Chapter 2
Proximities Revisited

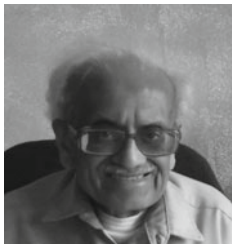

Fig. 2.1 Som Naimpally

This chapter takes another look at the very rich proximity landscape. An overview of the proximity landscape is given in the life and work of S.A. Naimpally (Som). For a recent picture of Som, see Fig. 2.1 and for an overview of Som's research contributions, see [1]. This is a remarkable story of a mathematician who began studying proximity space theory after he completed his Ph.D. as a result of a chance meeting at the University of Michigan between Som and a visitor from Cambridge University Press, who invited him to write a monograph on proximity. This he did together with his graduate student B.D. Warrack, leading to a complete overview of proximity space theory until 1970 [2].

The study of the nearness of sets now spans more than 100 years, starting with the address by F. Riesz at the International Congress of Mathematicians in Rome in 1908 [3], recently commented on by S.A. Naimpally [4, 5] and A. Di Concilio [6–8]. One of the earliest introductions to nearness (proximity) relations was given by E. Čech during a 1936–1939 Brno seminar, published in 1966 [9, Sect. 25.A.1]. Čech used the symbol p to denote a proximity relation defined on a nonempty set X, which Čech axiomatized. Čech's work on proximity spaces started two years after V.A. Efremovič's work (in 1933), who introduced a widely considered axiomatization of proximity, which was not published until 1951 [10]. For a detailed

J.F. Peters, *Computational Proximity*, Intelligent Systems
Reference Library 102, DOI 10.1007/978-3-319-30262-1_2

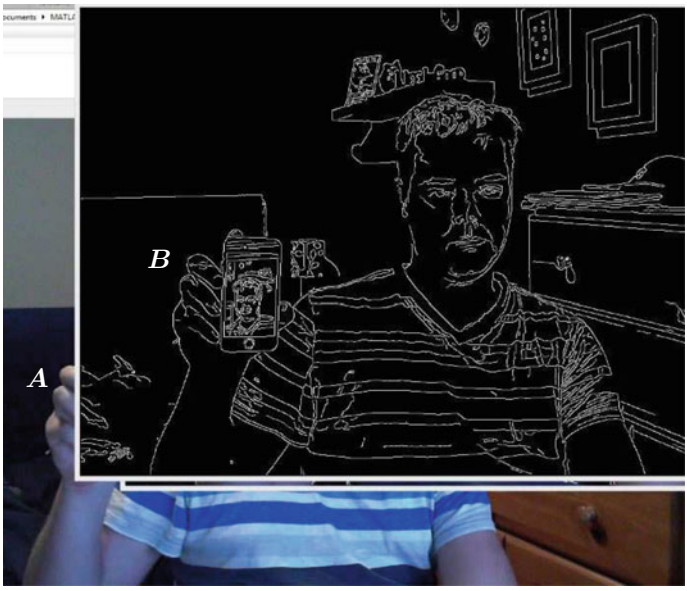

Fig. 2.2 $A\ \delta_{\Phi}\ B$ (descriptively near sets)

presentation of Efremovič's proximity axioms, see, e.g., [8, 11] and for applications, see, e.g., [12–16].

This chapter revisits a number of familiar proximities. It also introduces Delaunay triangulation and takes another look at Voronoï diagrams. The focus in this second look at proximities is on finite proximity spaces and the strong nearness of sets and points to sets. For example, let X be a finite topological space on the set of points in the digital image in Fig. 2.2 and let X be endowed with the descriptive Lodato proximity δ_{Φ}.

Let A be that part of Fig. 2.2 showing the hand and torso and let B be that part of the image showing detected edges.[1] Let a description $\Phi(A)$, $A \subset X$ be defined by the shape descriptor gradient orientation of the edge pixels in A. Clearly, $A\ \delta_{\Phi}\ B$, since, for instance, the gradient orientation of the edge pixels along the top edges of the hand in A are exactly the same as the gradient orientation of the edge pixelsalong the top edges of the hand in B. In fact, this is an example of strong descriptive nearness with $A\ \overset{\wedge\wedge}{\delta}_{\Phi}\ B$.

[1] Many thanks to Braden Cross for the webcam image in Fig. 2.2, captured using the Matlab Computer Vision System toolbox and Matlab implementation of the Canny edge detection algorithm.

2.1 Cech Proximity

A nonempty set X endowed with the Čech proximity relation δ is a proximity space, denoted (X, δ). *Distant* (*far*, *remote*) sets A, B are not near, denoted by $A \not\delta B$. In a metric topology endowed with a proximity, sets are remote, provided $D(A, B) > 0$. In a finite proximity space, remote sets can be defined without reference to a metric. That is, $A \not\delta B$, provided A and B have no points in common. Remote sets play an important role in applications of topology [14] and the topology of digital images [17]. That is, remote sets are disjoint, having no elements in common.

Remote sets are **separated sets** in any space. For example, separated sets of picture elements in the layered digital image in Fig. 2.2 correspond to the remote image regions such as the set of hand pixels A, which is separated from the set of hand edge pixels B. By identifying image regions remote from each other, we have a means of identifying separated image patterns, distinguishing one from the other by characteristics such as

1^o smooth, continous, thick region edges such as those in the hand region A in Fig. 2.2.

2^o non-smooth, fragmented, thin region edges such those in as in the hand region B in Fig. 2.2.

> Edgewise in Fig. 2.2, A and B are remote (edges are separated *spatially* and are different *descriptively*). Hence, we write $A \not\delta B$ (edges A are not close to edges B) and $A \not\delta_\Phi B$ (edges A are not descriptively the same as B). ■

3^o skin-colour hand with solid shapes and with highlighted (chiaroscuro) parts in region A in Fig. 2.2.

4^o white hand edge-enclosed shapes on a densely black background and with no highlighting (chiaroscuro) parts in region B in Fig. 2.2.

> Shape-wise in Fig. 2.2, A and B are remote (shapes are separated *spatially* and are different *descriptively*). Hence, again, we write $A \not\delta B$ (shape A is not close to shape B) and $A \not\delta_\Phi B$ (shape A is not descriptively the same as B). ■

The Čech proximity δ is the most elementary form of proximity relation. The relation δ (*close, near, proximal*) is a Čech proximity relation on the family of all subsets 2^X of X, provided it satisfies the axioms (**P1**)–(**P4**) given earlier in Sect. 1.4, introduced during the mid-1930s by E. Čech [9, Sect. 25, p. 439]. Let A, B be nonempty subsets in X. The expression $A \,\delta\, B$ reads A *close to* B and $A \not\delta B$ reads A *is not close to* B. Also recall that $\varnothing$ denotes the empty set. A set E is empty, provided E has no elements, members, points. The intersection of A and B (denoted by $A \cap B$) is the set of points that are common to (*in both*) A and B, i.e.

$$A \cap B = \{x \in A \cup B : x \in A \text{ and } x \in B\}.$$

Let X be a nonempty set, $x \in X$, $A, B \subset X$. The Čech proximity δ (or any of the other proximities in Sect. 1.4) can be used to define the closure of a set. Recall that

$$\mathrm{cl}B = \{x \in X : x \ \delta \ B\} \ \textbf{(Closure of a set)}.$$

The union of A and B (denoted by $A \cup B$) is the set of points that are in A or B. The Kuratowski [18] closure operator cl leads to refinements of each of the usual proximities.

Definition 2.1 Let X be a nonempty set, $A, B \subset X$. The *closure operator* is a self map on 2^X the power set of X (collection of all subsets of X) satisfies the following axioms.

K.1 $\mathrm{cl}\varnothing = \varnothing$.
K.2 $B \subset \mathrm{cl}B$.
K.3 $\mathrm{cl}(A \cup B) = \mathrm{cl}A \cup \mathrm{cl}B$.
K.4 $\mathrm{cl}(\mathrm{cl}B) = \mathrm{cl}B$.

The following axioms stem from finite sets.

K.5 If X is finite, then $\mathrm{cl}X = X$ (Kuratowski [18, Sect. 4, III]).
K.6 A subset $B \subset X$ is closed, if and only if $\mathrm{cl}B = B$.

For a brief overview of Kuratowski closure, see Appendix B. ■

From Axiom **K**.6, a subset B in X is **closed** if and only if B coincides with its closure, i.e., $\mathrm{cl}B = B$ [19].

Example 2.2 **Closed Sets**.
Let X be a finite subset in Euclidean space $\mathbb{R}^2$, $A, B, S \subset X$, $p, q, r \in S$. Further, let $\mathrm{bd}A$ denote the boundary of A, $\mathrm{int}A = A \setminus \mathrm{bd}$ the interior of A. Here are some examples of closed sets.

1^o Each region V_p in a Voronoï diagram $V(S)$ is a closed set, since $\mathrm{cl}V_p = V_p$ (from Axiom **K**.6). Every region V_p is a solid polygon with nonempty interior and includes its boundary.
2^o Each triangle $\triangle(pqr)$ in a Delaunay triangulation $D(S)$ is a closed set with an empty interior.
3^o In the psychology of human vision, it has been suggested that perceived objects always include their boundaries [20].
4^o **Regular closed**. A set A is **regular closed**, provided $A = \mathrm{cl}(\mathrm{int}A)$. On the other hand, a set A is **regular open**, provided $B = \mathrm{int}(\mathrm{cl}B)$. That is, a nonempty set is *open*, if it coincides with its interior of its closure. Notice that $B \subseteq A$.
5^o The description $\Phi(x)$ of a pixel x in a digital image A is a closed set, since each pixel can be completely described without reference to the description of its adjacent pixels, i.e., $\{\Phi(x)\} = \mathrm{cl}(\{\Phi(x)\})$. ■

Problem 2.3 Is a set $\{x\}$ containing a single pixel x in a digital image a regular open set? ■

If $A \subset X$ contains a single element $x \in X$, then, for simplicity, we write $x \ \delta \ B$ instead of $\{x\} \ \delta \ B$. That is, x is near B.

Then the closure axioms can be rewritten using the nearness relation between points and sets as in [19, Sect. 2]. This is done by defining $x \ \delta \ B \Leftrightarrow x \in \mathrm{cl}B$. In that case, the point x is near B. From this, we obtain the following Lodato point-set proximity axioms.

Definition 2.4 Lodato Point-Set Proximity Revisited.
Let X be a proximity space endowed with a proximity δ, $x \in X$, nonempty sets $A, B, C \subset X$. δ is point-set proximity, provided it satisfies the following axioms.
T.1 $x \ \delta \ B \Rightarrow B \neq \varnothing$
T.2 $x \cap B \neq \varnothing \Rightarrow x \ \delta \ B$ (uniformity).
T.3 $x \ \delta \ (B \cup C) \Leftrightarrow x \ \delta \ B$ or $x \ \delta \ C$.
T.4 $x \ \delta \ B$ and $b \ \delta \ C$ for each $b \in B \Rightarrow x \ \delta C$.
In addition, if X is finite, we have
T.5 $x \ \delta \ B \Leftrightarrow \mathrm{cl}x \cap \mathrm{cl}B \neq \varnothing$ (Wallman). ■

> A relation δ that satisfies Axiom **T**.2 is called a *discrete proximity* on the family of sets of X [8, Sect. 2.1, p. 93].

Further, if X is finite, we have

Theorem 2.5 *Let X be a finite Čech proximity space, $x, y \in X, x \neq \varnothing, B \subset X$. Then the following are equivalent.*
1^o $x \ \delta \ B$.
2^o $x \in B$ *implies* $x \cap B \neq \varnothing$.
3^o $clx \subset clB \Leftrightarrow \{x\} \subset B$.
4^o $cl(x \cap B) \subset (clx \cap clB) \subset x \cap B$

Proof
$1^o \Leftrightarrow 2^o$: $x \ \delta \ B \Leftrightarrow \mathrm{cl}x \cap \mathrm{cl}B \neq \varnothing$ (Axiom **T**.5) $\Leftrightarrow x \in B$ implies $x \cap B \neq \varnothing$.
$2^o \Leftrightarrow 3^o \Leftrightarrow 4^o$. □

Theorem 2.6 *Let X be a finite Čech proximity space, $x, y \in X, x \neq \varnothing, B \subset X$.*
1^o *Points x, y are remote, if and only if $clx \cap cly = \varnothing$.*
2^o *A point x is separated from B, if and only if $clx \cap clB = \varnothing$.*

Proof
1^o: Let $B = \{x\}$ and the result follows from Axiom **T**.5.
2^o: From Axiom **T**.5, $\mathrm{cl}x \cap \mathrm{cl}B = \varnothing \Leftrightarrow x \not\delta B$. □

Fig. 2.3 $x\ \delta_\Phi\ B$

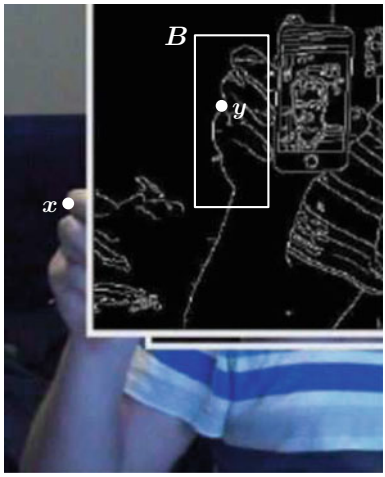

The **closure of a picture point** (digital image pixel or painting spot) equals the union of itself and its adjacent (boundary) points, i.e.,

$$
\begin{aligned}
X &= \text{ set of picture points.}\\
\|x-y\| &= 1, \text{ if and only if } x, y \text{ are } \textbf{adjacent}.\\
\text{bdy}(x) &= \{y \in X : y \text{ adjacent to } x\}.\\
\text{cl}x &= \text{bdy}(x) \cup \{x\} \text{ (Closure of picture point).}
\end{aligned}
$$

Remote picture points are those points that do not have common adjacent points.

Definition 2.7 Types of Remote Picture Points.
Let X be a finite set of picture points endowed with proximities δ, δ_Φ. Two basic types of remote picture points can be found in X.

1^o **Spatially remote points**. *Spatially remote picture points* are those points that do not have common adjacent points.

2^o **Descriptively remote points**. Descriptively remote picture points are those points that do not have matching descriptions. Notice that adjacent points can be descriptively remote. ■

Example 2.8 **Remote Picture Points**.
Let X be a finite set of picture points in Fig. 2.3 endowed with proximities δ, δ_Φ, $x, y \in X$. Then x is spatially remote from y, i.e., $x\ \not\delta\ y$, since $\text{cl}x\ \not\delta\ \text{cl}y$. Assuming that x and y have the different gradient orientations, x is descriptively remote from y, i.e., $x\ \not\delta_\Phi\ y$. ■

Example 2.9 **Descriptive Nearness of Points to Sets: Finite Case**.
Let X be a finite descriptive point-set proximity space (X, δ_Φ) that consists of the picture points shown in Fig. 2.3, B be the finite set of hand-edge picture points in Fig. 2.3, $x \in X$. The picture point x lies on the outer edge of the hand image and B is restricted to the set of edge picture points in Fig. 2.3. Assume that each picture point is described by its gradient orientation. In that case, $x \; \delta_\Phi \; B$, since the gradient orientation of x matches the gradient orientation of at least one of the picture points in B. ■

Definition 2.10 Types of Close Picture Points.
Let X be a finite set of picture points endowed with proximities δ, δ_Φ. Several basic types of close picture points can be found in X.

1^o **Spatially close points**. *Spatially close picture points* are those points that are adjacent.

2^o **Strongly close point to a set**. A picture point x **Strongly close** to a set $A \subset X$ is a member of A, i.e., $x \in A$ and $x \; \overset{\Lsh}{\delta} \; A$.

3^o **Descriptively close points**. *Descriptively close picture points* are those points that have matching descriptions, i.e., $\Phi(x) \in \Phi(A)$ (description of x belongs to the set of descriptions of the points in A. Notice that spatially remote points can be descriptively close). ■

Example 2.11 **Near and Strongly Near Picture Points**.
Let X be a finite set of picture points in Fig. 2.3 endowed with proximities δ, δ_Φ, $x, y \in X$. Then x is spatially close to all of is adjacent points. The point y is strongly close to B, i.e., $y \; \overset{\Lsh}{\delta} \; B$, since $y \in B$. From Example 2.9, the point x is descriptively close to at least one edge point in B. ■

Example 2.12 **Near Polygons**.
Polygons A and B in Fig. 2.4 are examples of Voronoï regions in the mesh on hand image.[2] A and B have a common edge, $\mathrm{cl}A \cap \mathrm{cl}B \neq \varnothing$. Hence, from Axiom prox.2, $A \; \delta \; B$, i.e., A is close to B. In fact, $A \; \overset{\Lsh}{\delta} \; B$, since $\mathrm{cl}A \cap \mathrm{cl}B$ contains more than one point.

Every point in the common edge shown in Fig. 2.4 is strongly near both A and B, since A and B overlap. All points y in A not on the common edge are spatially remote from B, i.e., $y \; \not\delta \; B$. The point x labeled with a red dot ● in A is descriptively near the point y labeled with a red dot ● in B, provided $\Phi(x) = \Phi(y)$. In that case, $x \; \overset{\Lsh}{\delta_\Phi} \; B$, since $\Phi(x) \in \Phi(B)$, x is strongly close descriptively to B, since, by assumption, the description of x belongs to the set of descriptions of the points in B. ■

Remark 2.13 From this point forward, assume that δ is the Wallman proximity. ■

[2]Many thanks to Binglin Li for this hand image in Fig. 2.4.

Fig. 2.4 $A \overset{\wedge}{\delta} B$

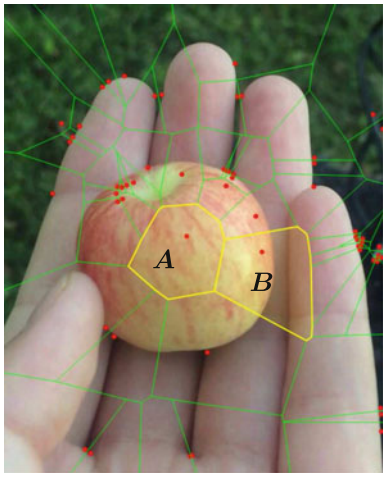

Problem 2.14 Let X be the set of polygons in the Voronoï mesh on the hand image in Fig. 2.4. Let δ be a nearness (proximity) relation on X. Prove that each of the Čech axioms are satisfied by δ. In effect, prove that δ is the Čech proximity and that (X, δ) is an example of a Čech proximity space.
Hint: From Example 2.12, we know that δ satisfies Axiom prox.2. So it is only necessary to prove that the remaining three Čech axioms are satisfied. ■

2.2 Cech Closure of a Set

From the Čech proximity relation δ, we can derive the closure of a nonempty set [9]. Recall that the closure of a set A (denoted cl$A$) is the union of its interior points (denoted int$A$) and its boundary points (denoted bdy$A$). In fact, in a proximity space, the closure of a set A is the union of all points near A. Hence, the earlier formulation of the closure of nonempty set is rewritten in terms of the union of all of its near points. In a proximity space X, the *closure* of a subset $A \subset X$ is defined by

$$\text{cl}A = \bigcup_{x \in X} \{x \ \delta \ A\} \text{ (closure of the set } A).$$

This formulation of the closure of a set is one of the properties of a proximity space[3] introduced by V.A. Efremovič [10]. The space (X, cl) is called a *closure space*. A point is *proximal* in (X, cl) if and only if $x \in \text{cl}X$. The closure of a set X contains all points proximal to X. In a proximity space with the closure property, δ is called a *Wallman proximity*, named after H. Wallman [21].

[3]Pointed out by I. Dochviri.

Let subsets $A, B \subset X$, which is a proximity space. The negative of the Wallman proximity is very interesting, since it paves the way for the study of the separation of structures, i.e., those that have no points in common. That is,

$$A \not\delta B, \text{ if and only if } \mathrm{cl}A \cap \mathrm{cl}B = \varnothing.$$

Wallman proximity is particularly important in finding hidden patterns in digital images, especially if we are comparing and contrasting geometric structures such as edges, corners, line segments and other convex polygons in images.

2.3 Near Edge Sets

A set endowed with a proximity relation is called a proximity space. A *relator* is a nonvoid family of relations $\mathcal{R}$ on a nonempty set X. The pair $(X, \mathcal{R})$ (also denoted $X(\mathcal{R})$) is called a relator space. Sets A, B are descriptively near (have descriptive proximity), provided there are one or more pairs of points $a \in A, b \in B$ with matching descriptions.

Example 2.15 In Fig. 2.5, sets A_1, A_2, M' have EF-proximity (spatially near), since these sets have points in common. That is, $A_1 \ \delta \ M', A_2 \ \delta \ M', A_1 \ \delta \ A_2$. Sets A_1, A_2, B_1, B_2, M' have descriptive proximity (descriptively near), since one can find pairs of points with matching descriptions. All of these sets contain black edge points. That is, $A_1 \ \delta_\Phi \ M', \ A_2 \ \delta_\Phi \ M', A_1 \ \delta_\Phi \ A_2$ and $A_1 \ \delta_\Phi \ B_1, A_2 \ \delta_\Phi \ B_2, B_1 \ \delta_\Phi \ B_2$ and so on. ■

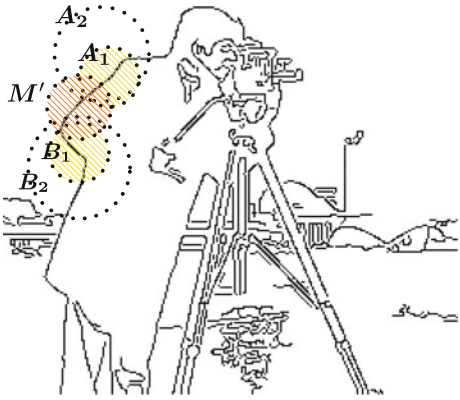

Fig. 2.5 Near edge sets

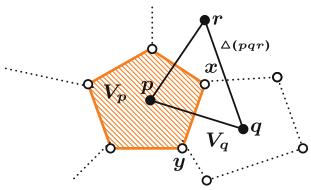

Fig. 2.6 Delaunay triangle $\triangle(pqr)$

2.4 Lodato Proximity

Recall how a *Lodato proximity* is defined [22–24] (see, also, [5, 11]). Let X be a nonempty set. A *Lodato proximity* δ is a relation on $\mathscr{P}(X)$ which satisfies the following axioms for all subsets A, B, C of X:

Lodato Proximity Axioms

(P0) $\varnothing \not\delta A, \forall A \subset X.$
(P1) $A \ \delta \ B \Leftrightarrow B \delta A.$
(P2) $A \cap B \neq \varnothing \Rightarrow A \delta B.$
(P3) $A \ \delta \ (B \cup C) \Leftrightarrow A \ \delta \ B$ or $A \ \delta \ C.$
(P4) $A \ \delta \ B$ and $\{b\} \ \delta \ C$ for each $b \in B \ \Rightarrow A \ \delta \ C.$ ■

Further δ is *separated* , if

(P5) $\{x\} \ \delta \ \{y\} \Rightarrow x = y.$ ■

We can associate a topology with the space (X, δ) by considering as closed sets the ones that coincide with their own closure, where for a subset A we have

$$\mathrm{cl}A = \{x \in X : x \ \delta \ A\}.$$

This is possible because of the correspondence of the Lodato axioms with the well-known Kuratowski closure axioms (see Appendix B).

Example 2.16 **Lodato proximal Cameraman Elbow Sets**.
Let (X, δ) be a Lodato proximity space represented by set of points in the partial cameraman image in Fig. 2.7, $A_1, A_2, M', B_1, B_2 \subset X$. The Lodato axiom **(P4)** is satisfied by

$$M' \ \delta \ A_1, \ A_1 \ \delta \ A_2 \forall a \in A_1 \Leftrightarrow M' \ \delta \ A_2,$$
$$M' \ \delta \ B_1, \ B_1 \ \delta \ B_2 \forall b \in B_1 \Leftrightarrow M' \ \delta \ B_2.$$ ■

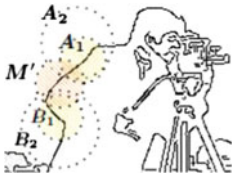

Fig. 2.7 Proximal cameraman elbow sets

2.5 Descriptive Lodato Proximity

Descriptive Lodato proximity was introduced in [17]. Let X be a nonempty set, $A, B \subset X, x \in X$. Recall that $\Phi(x)$ is a feature vector that describes x, $\Phi(A)$ is the set of feature vectors that describe points in A. The descriptive intersection between A and B (denoted by $A \underset{\Phi}{\cap} B$) is defined by

$$A \underset{\Phi}{\cap} B = \{x \in A \cup B : \Phi(x) \in \Phi(A) \text{ and } \Phi(x) \in \Phi(B)\}.$$

A *Descriptive Lodato proximity* δ_Φ is a relation on $\mathscr{P}(X)$ which satisfies the following axioms for all subsets A, B, C of X, which is a descriptive Lodato proximity space:

Descriptive Lodato Proximity Axioms Revisited

(dP0) $\varnothing \not\delta_\Phi A, \forall A \subset X$.
(dP1) $A \ \delta_\Phi \ B \Leftrightarrow B \ \delta_\Phi \ A$.
(dP2) $A \underset{\Phi}{\cap} B \neq \varnothing \Rightarrow A \ \delta_\Phi \ B$.
(dP3) $A \ \delta_\Phi \ (B \cup C) \Leftrightarrow A \ \delta_\Phi \ B$ or $A \ \delta_\Phi \ C$.
(dP4) $A \ \delta_\Phi \ B$ and $\{b\} \ \delta_\Phi \ C$ for each $b \in B \Rightarrow A \ \delta_\Phi \ C$. ■

Further, the Lodato space (X, δ_Φ) **descriptively separated**, if, for $x, y \in X$,

(dP5) $\{x\} \ \delta_\Phi \ \{y\} \Rightarrow \Phi(x) = \Phi(y)$ (x and y have matching descriptions). ■

Example 2.17 **Descriptive Lodato Proximity on Apple Sets**.
Let (X, δ) be a Lodato proximity space represented by set of points in the partial image of an apple in Fig. 2.8, with subsets $I, J, A, K, B \subset X$. The Lodato axiom **(P4)** is satisfied by

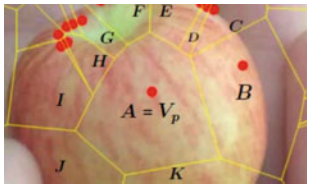

Fig. 2.8 Descriptive Lodato near apple sets

$$I\ \delta_\Phi\ A,\ A\ \delta_\Phi\ B \forall\ \Phi(a) \in \phi(A) \Leftrightarrow I\ \delta_\Phi\ B,$$
$$H\ \delta_\Phi\ A,\ A\ \delta_\Phi\ B \forall\ \Phi(a) \in \phi(A) \Leftrightarrow H\ \delta_\Phi\ B. \quad \blacksquare$$

2.6 Delaunay Triangulation

Delaunay triangulations, introduced by B.N. Delone [Delaunay] [25], represent pieces of a continuous space. This representation supports numerical algorithms used to compute properties such as the density of a space. A *triangulation* is a collection of triangles, including the edges and vertices of the triangles in the collection. A 2D *Delaunay triangulation* of a set of sites (generators) $S \subset \mathbb{R}^2$ is a triangulation of the points in S. Let $p, q \in S$. A straight edge connecting p and q is a *Delaunay edge* if and only if the Voronoï region of p [26, 27] and Voronoï region of q intersect along a common line segment [28, Sect. I.1, p. 3]. For example, in Fig. 2.6, $V_p \cap V_q = \overline{xy}$. Hence, $\overline{pq}$ is a Delaunay edge in Fig. 2.6.

A triangle with vertices $p, q, r \in S$ is a *Delaunay triangle* (denoted $\triangle(pqr)$ in Fig. 2.9), provided the edges in the triangle are Delaunay edges.

Example 2.18 **Near Sets in a Delaunay Triangulation**.
A *triangulation* is a collection of triangles, including the edges and vertices of the triangles in the collection. A 2D *Delaunay triangulation* of a set of sites (generators) $S \subset \mathbb{R}^2$ is a triangulation of the points in S, forming a collection of Delaunay triangles $\mathcal{D}$. Also let $\mathcal{D}$ be endowed with the Čech proximity δ. Let A, B be sets of points along the edges of the Delaunay triangles $\triangle(pqr)$ and $\triangle(qrt)$ in Fig. 2.9. $A \cap B \neq \varnothing$, since this pair of triangles have a common edge. Hence, $A\ \overset{\lll}{\delta}\ B$. In addition, $(\mathcal{D}, \delta)$ is called a Delaunay proximity space [29]. $\blacksquare$

Example 2.19 **Image Corners**.
The hand image in Fig. 2.10.1 has dimension 552×685. This is reflected in the plot of the image corners in Fig. 2.11. Up to 50 corners were found in the hand image using MScript 27 in Appendix A.2. The corners are displayed as ● dots in Fig. 2.10.1. These corners form a set of sites that can be used to generate a Delaunay mesh. By connecting each pair of nearest sites belonging to neighbouring Voronoï regions, the

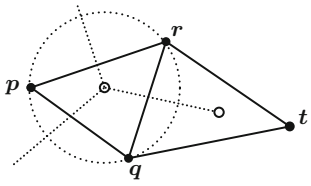

Fig. 2.9 Strongly near Delaunay triangles $\triangle(pqr)$ and $\triangle(qrt)$

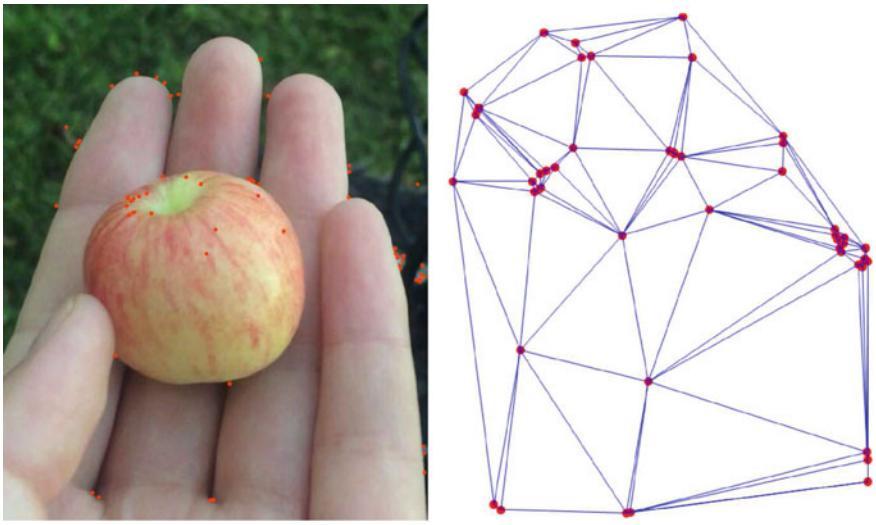

2.10.1: Delaunay mesh 2.10.2: Corner Locations

Fig. 2.10 Corner-based Delaunay mesh and corresponding image corners

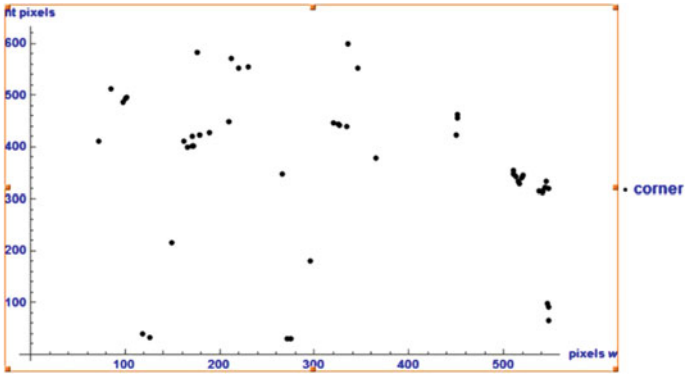

Fig. 2.11 Corners in a hand image

mesh in Fig. 2.10.2 is constructed. The locations of the Delaunay mesh corners are shown in the plot in Fig. 2.11. For the most part, the corners in the plot follow the contour of the hand (polygon A in Fig. 2.4 has the highest number of $\hat{\delta}$-neighbouring polygons). ■

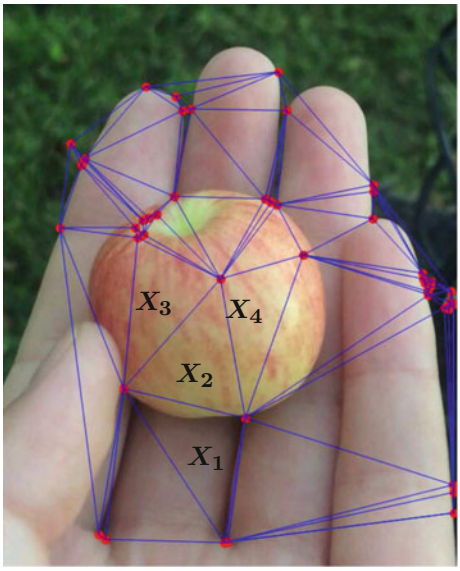

Fig. 2.12 Corner-based Delauny mesh on a hand image

Example 2.20 **Near and Strongly Near Delaunay Mesh Triangles**.
The corner-based Delaunay mesh in Fig. 2.10.2 is superimposed on the hand image in Fig. 2.12. This superimposition of a mesh on an image facilitates image analysis, since neighbouring triangles are then associated with image regions. In Fig. 2.12, let the set $X = \bigcup X_i, i \in \{1, 2, 3, 4\}$. Then the following things can be observed.

$$\begin{aligned}
&\mathrm{cl}X_1 \ \delta_0 \ \mathrm{cl}X_3, \ \text{Wallman proximity.}\\
&\mathrm{cl}X_1 \ \delta_0 \ \mathrm{cl}X_4, \ \text{Wallman proximity.}\\
&\mathrm{cl}X_1 \ \overset{\ll}{\delta} \ \mathrm{cl}X_3, \ \text{strong proximity.}\\
&\mathrm{cl}X_2 \ \overset{\ll}{\delta} \ \mathrm{cl}X_3, \ \text{strong proximity.}\\
&\mathrm{cl}X_2 \ \overset{\ll}{\delta} \ \mathrm{cl}X_4, \ \text{strong proximity.}\\
&X \text{ is connected.}\\
&X \text{ is a mesh nerve.}
\end{aligned}$$

The fact that X is connected and a mesh nerve is of interest, since this nerve sits on top of that part of the underlying Voronoï mesh containing a polygon that has the greatest number of adjacent polygons. ■

MScript 27 in Appendix A.2 is also used to construct the corner-based Voronoï mesh in Fig. 2.13.1 and the corresponding mesh is superimposed on the hand image in Fig. 2.13.2. The Voronoï regions of corner points grouped around the contour of the and the apple held in the hand, lay underneath the Delaunay nerve that includes $X4$ in Fig. 2.12.

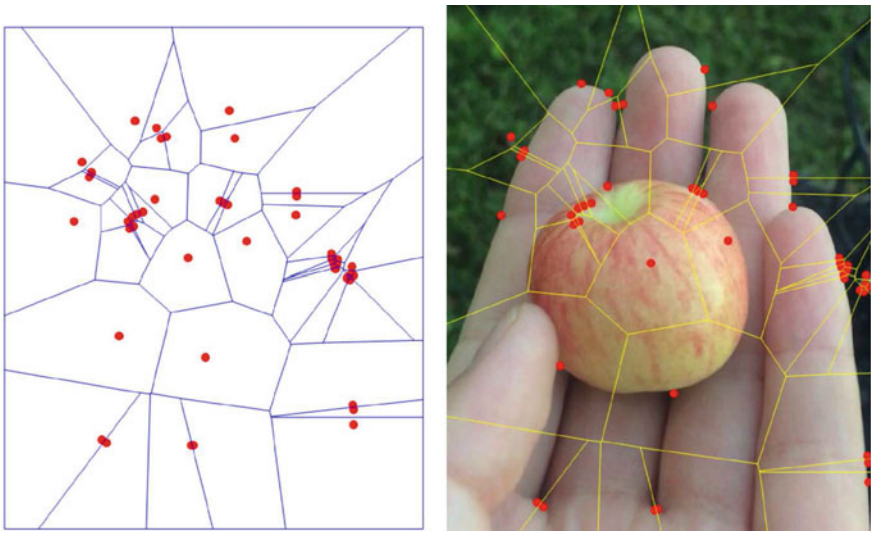

2.13.1: Voronoï mesh 2.13.2: Mesh on Image

Fig. 2.13 Corner-based Voronoï mesh and corresponding image mesh

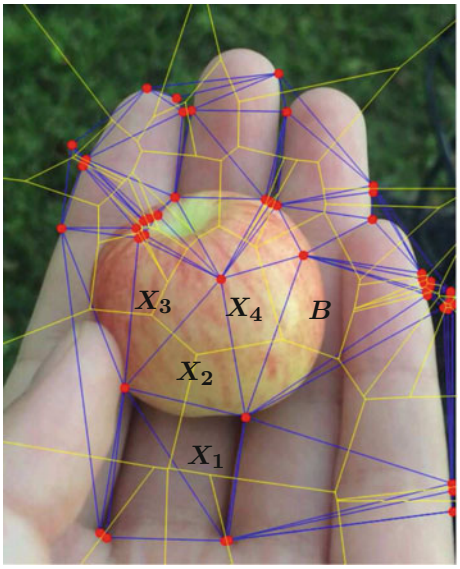

Fig. 2.14 Combined corner-based Voronoï and Delaunay meshes on a hand image

Example 2.21 **Delaunay Triangle-Voronoï Mesh Connectedness**.
The combined corner-based Voronoï and Delaunay image meshes in Fig. 2.14 are connected but not strongly connected. Triangles X_4 and B in Fig. 2.14 correspond to Voronoï regions A and B in Fig. 2.4. ■

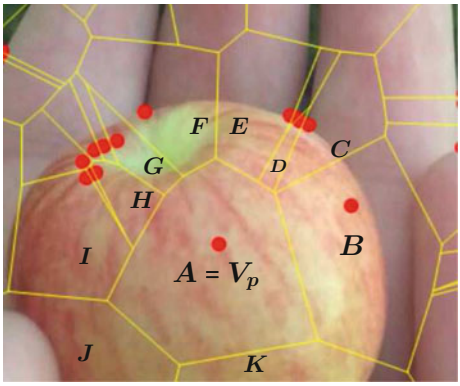

Fig. 2.15 Hand image Voronoï mesh nerve

Theorem 2.22 *A Delaunay triangle with a straight edge between a pair of Voronoï region sites is Wallman near but not* $\overset{\wedge\wedge}{\delta}$*-near to the pair of Voronoï regions.*

Problem 2.23 🚲 Prove Theorem 2.22. **Hint**: Use the fact that a Delaunay triangle has an empty interior, cuts each neigbouring Voronoï edge in only one point on the edge common to a pair of Voronoï regions. ■

Example 2.24 **Voronoï Mesh Closure Nerve**.
In Fig. 2.12, let X be the set of labelled Voronoï regions shown in Fig. 2.15, i.e.,

$$X = \bigcup X_i : X_i \in \{V_p, B, C, D, E, F, G, H, I, J, K\}. \text{(Set of adjacent Voronoï regions)}$$

Then the following things can be observed.

$$\begin{aligned} &\mathrm{cl}A\ \delta_0\ \mathrm{cl}X_i \forall X_i \in X, \text{ Wallman proximity.}\\ &A\ \overset{\wedge\wedge}{\delta}\ X_i \forall X_i \in X, \text{ strong proximity.}\\ &\bigcap \mathrm{cl}X \neq \varnothing.\\ &X \text{ is a mesh closure nerve.}\\ &X \text{ is not connected, since,e.g., } \mathrm{cl}B \cap \mathrm{cl}E = \varnothing.\\ &X \text{ is not a bornology, since } X \text{ is not a boundedness.} \end{aligned}$$

X is a mesh closure nerve that has nonempty intersection with a Delaunay mesh closure nerve. ■

Problem 2.25 Prove the set X in Example 2.24 is a mesh closure nerve. ■

Problem 2.26 Prove the set X in Example 2.24 is not connected. ■

Problem 2.27 Prove the set X in Example 2.24 is not a bornology. ■

2.7 Voronoï Diagrams Revisited

This section revisits Voronoï diagrams, introduced during the first decade of the 1900s by G. Voronoï [30–32]. A *simple convex set* is a closed half plane (all points on or on one side of a line in R^2).

Let $S \subset \mathbb{R}^2$ be a finite set of n points called sites, $p \in S$. The set S is called the *generating set* [33]. Let H_{pq} be the closed half plane of points at least as close to p as to $q \in S \setminus \{p\}$, defined by

$$H_{pq} = \left\{ x \in R^2 : \|x - p\| \underset{q \in S}{\leq} \|x - q\| \right\}.$$

A *convex polygon* is the intersection of finitely many half-planes [28, Sect. I.1, p. 2]. See, for example, Fig. 2.16.

Remark 2.28 The Voronoï region V_p depicted as the intersection of finitely many closed half planes in Fig. 2.16 is a variation of the representation of a Voronoï region in the monograph by H. Edelsbrunner [26, Sect. 2.1, p. 10], where each half plane is defined by its outward directed normal vector. The rays from p and perpendicular to the sides of V_p are comparable to the lines leading from the center of the convex polygon in G.L. Dirichlet's drawing [34, Sect. 3, p. 216]. ■

2.7.1 Sites

Let $S \subset E$, a finite-dimensional normed linear space. Elements of S are called sites (mesh generating points) to distinguish them from other points in E [26, Sect. 2.2, p. 10]. Let $p \in S$. A *Voronoï region* of $p \in S$ (denoted V_p) is defined by

$$V_p = \left\{ x \in E : \|x - p\| \underset{\forall q \in S}{\leq} \|x - q\| \right\}.$$

Remark 2.29 A Voronoï region of a site $p \in S$ contains every point in the plane that is closer to p than to any other site in S [33, Sect. 1.1, p. 99]. Let V_p, V_q be Voronoï

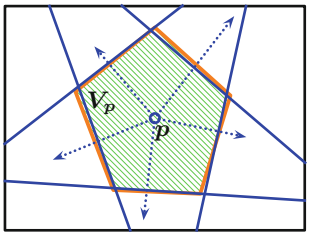

Fig. 2.16 Voronoï region = convex polygon

polygons. If $V_p \cap V_q$ is a line, ray or line segment, then it is called a *Voronoï edge*. If the intersection of three or more Voronoï regions is a point, that point is called a *Voronoï vertex*. ■

Lemma 2.30 *A Voronoï region of a point is the intersection of closed half planes and each region is a convex polygon.*

Proof From the definition of a closed half-plane

$$H_{pq} = \left\{ x \in R^2 : \|x - p\| \underset{q \in S}{\leq} \|x - q\| \right\},$$

V_p is the intersection of closed half-planes H_{pq}, for all $q \in S - \{p\}$ [28], forming a polygon. From Lemma 1.42, V_p is a convex. □

A Voronoï diagram of S (denoted by $\mathbb{V}$) is the set of Voronoï regions, one for each site $p \in S$, defined by

$$\mathbb{V} = \bigcup_{p \in S} V_p.$$

Example 2.31 **Centroids as Sites in an Image Tessellation**.
Let E be a segmentation of a digital image and let $S \subset E$ be a set of sites, where each site is the centroid of a segment in E. In a centroidal approach to the Voronoï tessellation of E, a Voronoï region V_p is defined by the intersection of closed half plains determined by centroid $p \in S$. Centroids can be found using **regionprops** available in Matlab®. The centroidal approach to Voronoï tessellation was introduced by Q. Du, V. Faber, M. Gunzburger [35]. ■

2.8 Some Results for Voronoï Regions

Let V_p, V_z be Voronoï regions of $p, z \in S$, a set of Voronoï sites in a finite-dimensional normed linear Space E that is topological, cl$A$ the closure of a nonempty set A in E. V_p, V_z are *proximal* (denoted by $V_p \ \delta \ V_z$), provided $\mathbb{P} = \text{cl}V_p \cap \text{cl}V_z \neq \varnothing$ [8]. The set $\mathbb{P}$ is called a *proximal Voronoï region*.

Theorem 2.32 *Proximal Voronoï regions are convex polygons.*

Proof Let $\mathbb{P}$ be a proximal Voronoï region. By definition, $\mathbb{P}$ is the nonempty intersection of convex sets. From Lemma 1.42, $\mathbb{P}$ is convex. Consequently, $\mathbb{P}$ is the intersection of finitely many closed half planes. Hence, from Lemma 2.30, $\mathbb{P}$ is a Voronoï region of a point and is a convex polygon. □

Corollary 2.33 *The intersection of proximal Voronoï regions is either a Voronoï edge or Voronoï point.*

Any two adjacent Voronoï regions intersect along one of their boundaries and have at most one edge in common. Together, the complete set of Voronoï regions $\mathbb{V}$ cover the entire plane [28, Sect. 2.2, p. 10]. For a set of sites $S \subset E$, a Voronoï diagram $\mathbb{D}$ of S is the set of Voronoï regions, one for each site in S.

Corollary 2.34 *A Voronoï diagram* $\mathbb{D}$ *equals* $\mathbb{V}$.

The partition of a plane E with a finite set of n sites into n Voronoï polygons is known as a Dirichlet tessellation, named after G.L. Dirichlet [36] (see [34]). A *cover* (covering) of a space X is a collection $\mathcal{U}$ of subsets of X whose union contains X (i.e., $\mathcal{U} \supseteq X$) [37, Sect. 15], [14, Sect. 7.1].

Corollary 2.35 *A Dirichlet tessellation* $\mathbb{D}$ *of the Euclidean plane* E *is a covering of* E.

Using Mathematica script 1, we detect the edges in the cameraman image shown in Fig. 2.17.

Mscript 1 Detecting Image Edges.

$img =$  ;

2.17.1: Cameraman

2.17.2: Edges

Fig. 2.17 Cameraman edges detected

***edges* = *EdgeDetect*[*img*, 5]** ■

Using Mathematica script 2, we obtain a Dirichlet tessellation of the cameraman image shown in Fig. 2.18.

Mscript 2 Dirichlet Tessellation.

***imgBounds* = *Transpose*[{{0, 0}, *ImageDimensions*[*img*]}];**

***vm* = *VoronoiMesh*[*ImageValuePositions*[*edges*, *White*], *imgBounds*]**
***HighlightMesh*[*vm*, *Style*[2, *Opacity*[0.1], *Yellow*]]** ■

Example 2.36 **Sample Dirichlet Tessellation of an Image**.
A sample covering of an image with Voronoï regions is accomplished with Mathematica10® by first detecting the main edges in an image and then using points along image edges as the sites in a Dirichlet tessellation of a selected image. For example, Mscript 1 to find the edges in the cameraman image (see Fig. 2.17). Then Mscript 2 is used to tessellate the edges in the cameraman image (see Fig. 2.18). ■

Recall that the Euclidean space $E = R^2$ is a metric space. The topology in a metric space results from determining which points are close to each set in the space. A point $x \in E$ is close to $A \subset E$, provided the Hausdorff distance $d(x, A) = inf\{\|x - a\| : a \in A\} = 0$. Let X, Y be a pair of metric spaces, $f : X \longrightarrow Y$ is a function such that for each $x \in X$, there is a unique $f(x) \in Y$. A continuous function preserves the closeness (proximity) between points and sets, i.e., $f(x)$ is

2.18.1: Dirichlet1

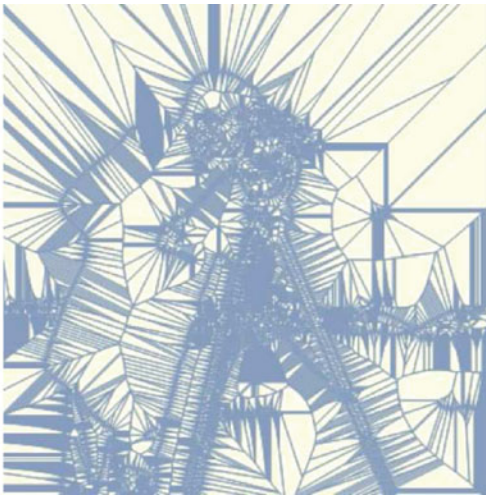

2.18.2: Dirichlet2

Fig. 2.18 Dirichlet tessellation of the cameraman image

close to $f(B)$ whenever x is close to B. In a proximity space, one set A is near another set B, provided $A\ \delta\ B$, i.e., the closure of A has at least one element in common with the closure of B. The set A is close to the set B, provided the Čech distance $D(A, B) = inf\{\|a - b\| : a \in A, b \in B\} = 0$. In that case, we write $A\ \delta\ B$ (A and B are proximal). A *uniformly continuous mapping* is a function that preserves proximity between sets, i.e., $f(A)\ \delta\ f(B)$ whenever $A\ \delta\ B$. A *Leader uniform topology* is determined by finding those points that are close to each given set in E.

Theorem 2.37 *Let S be a set of two or more sites, $p \in S$, $V_p \in \mathbb{D}$ in the Euclidean space R^2. Then*

1^o V_p is near at least one other Voronoï region in $\mathbb{D}$.
2^o Let p, y be sites in S. $\{y\}\ \delta\ \{p\} \Rightarrow \{y\}\ \delta\ V_p$.
3^o V_p is close to Voronoï region V_y if and only if $d(x, V_y) = 0$ for at least one $x \in V_p$.
4^o A mapping $f : V_p \longrightarrow V_y$ is uniformly continuous, provided $f(V_p)\ \delta\ f(V_y)$ whenever $V_p\ \delta\ V_y$.

Proof
1^o: Assume S contains at least 2 sites. Let $p \in S$, $y \in S \setminus \{y\}$ such that V_p, V_y have at least one closed half plane in common. Then $V_p\ \delta\ V_y$.
2^o: If $\{y\}\ \delta\ \{p\}$, then $\|y - p\| = 0$, since $y \in \{y\} \cap \{p\}$. Consequently, $\{y\} \cap \text{cl}(V_p) \neq \varnothing$ Hence, $\{y\}\ \delta\ \text{cl}(V_p)$.
3^o: $V_p\ \delta\ V_y \Leftrightarrow$ exists $x \in \text{cl}(V_p) \cap \text{cl}(V_y) \Leftrightarrow d(x, V_y) = 0$.
4^o: Let $f(V_p)\ \delta\ f(V_y)$ whenever $V_p\ \delta\ V_y$. Then, by definition, $f : V_p \longrightarrow V_y$ is uniformly continuous. □

Theorem 2.38 *Every collection of proximal Voronoï regions has a Leader uniform topology (application of* [38]*).*

Proof Assume $\mathbb{D}$ has more than one Voronoï region. For each $V_p \in \mathbb{D}$, find all $V_y \in \mathbb{D}$ that are close to V_p. For each V_p, this procedure determines a family of Voronoï regions that are near V_p. Let τ be a collection of families of proximal Voronoï regions. Let $A, B \in \tau$. $A \cap B \in \tau$, since either $A \cap B = \varnothing$ or, from Theorem 2.37.1^o, there is at least one Voronoï region $V_p \in A \cap B$, i.e., $V_p\ \delta\ A$ and $V_p\ \delta\ B$. Hence, $A \cap B \in \tau$. Similarly, $A \cup B \in \tau$, since $V_p\ \delta\ A$ or $V_p\ \delta\ B$ for each $V_p \in A \cup B$. Also, $\mathbb{D}, \varnothing$ are in τ. Then, τ is a Leader uniform topology in $\mathbb{D}$. □

2.9 Dirichlet Tessellation Quality and Digital Image Quality

The choice of sites influences the quality of the cells in a Dirichlet tessellations (Voronoï diagrams) [39]. Let X be a nonempty set of polygons in a Dirichlet tessellation, $x, y \in X$. A polygon $x \in X$ in a tessellation is called a **cell**. A number of cell quality measures are reported by J.R. Shewchuk in [40, Sect. 6.3]. A **fair** (**quality**) measure $\mathcal{Q} : X \longrightarrow \mathbb{R}$ satisfies the following axioms.

Q.1 $\mathcal{Q}(x) = 0$ for 2D cells with zero area.
Q.2 $\mathcal{Q}(x) = \mathcal{Q}(y)$ if and only if the 2D cells x and y are similar.
Q.3 $\mathcal{Q}(x)$ is finite.
Q.4 $\mathcal{Q}(x) \in [0, 1]$.

Let S be a set of tessellation cells, A the area of a tessellation containing a 3-sided polygon cell $s \in S$, l_1, l_2, l_3 the lengths of the sides of s with $Q(s)$ the quality of cell s. Then, for example, R.P. Bhatia and K.L. Lawrence [41], R.E. Bank and J. Xu [42] as well as D.A. Field [43] use the following smooth quality measure of a 3-sided cell.

$$Q_3(s) = 4\sqrt{3}\frac{A}{l_1^2 + l_2^2 +, l_3^2}.$$

Field observes, for triangles with vertices at (0,0), (1,0) and (x, y), $x \geq 0$, $y > 0$, we have

$$Q_3(s) = \frac{4\sqrt{3}y}{1 + (1 - x)^2 + 2y^2 + x^2}.$$

Problem 2.39 What does a high quality Dirichlet tessellation of a digital image tell us about the image? **Hint**: See introduction to convex bodies and Helly's theorem, starting in Chap. 11. ■

Problem 2.40 Do the following:

1^o Prove that $Q_3(s)$ satisfies the axioms for a fair measure of triangular tessellation cell quality.
2^o Plot $Q_3(s)$ for triangles with vertices at (0,0), (1,0) and (x, y) for fixed $x \geq 0$ and varying $y > 0$. ■

Problem 2.41 Do the following:

1^o Give a fair measure $Q_4(s)$ that satisfies the axioms for a fair measure of a 4-sided tessellation cell quality.
2^o Prove that your $Q_4(s)$ satisfies the fair measure axioms.
3^o For fixed 4gon lengths l_1, l_2, l_3, varying area A and varying length l_4, plot $Q_4(s)$ for 5 different values of A and l_4.
4^o For fixed 4gon lengths l_1, l_2, varying area A and varying lengths l_3, l_4, plot $Q_4(s)$ for 5 different values of A and l_3, l_4. ■

Let $l_1, l_2, \ldots, l_n$ be the lengths of the edges of an n-sided tessellation polygon. It has been shown that mesh quality is maximum, provided $l_1 = l_2 = \cdots = l_n$ [39, Sect. 5, Theorem 5.1]. When a digital image is the source of sites for tessellation, then tessellation quality tells us about the quality of the image. This observation can be used to prove Theorem 2.42.

Theorem 2.42 Mesh Quality [39].
For any plane, there exists a set of sites for which the mesh quality is maximum.

Problem 2.43 Do the following:

1^o Prove Theorem 2.42.
2^o Select three digital images.
3^o Select several different sets of sites on each of the images. Include centroidal and keypoint sites in your choices of sites.
4^o Tessellate the selected with image with Voronoï diagrams using the selected sites.
5^o Use Mathematica to measure the quality of the tessellated images.
6^o Give the quality measurement for each of the tessellated images.
7^o Comment on why one choice of sites leads to a higher quality tessellation than the other choices of sites. ■

Support for Image Object Geometry and Analysis.
When the Voronoï regions in a tessellated digital image have sides approaching equal length, then any line segment in any direction inside a Voronoï region can be used to identify and measure the geometry of image objects covered by the Voronoï region. ■

Example 2.44 **Digital Image Quality.**
For Fig. 2.19, let ⌜Centroids denotes sites that centroids that are also corners and let $\overline{\wedge}$Centroids denoted centroids that are also edge pixels. In this example, if the sites for a tessellation are image ⌜Centroids, then the quality of the image is a function of the number of centroid-corners, the positions of the centroid-corners and how evenly the

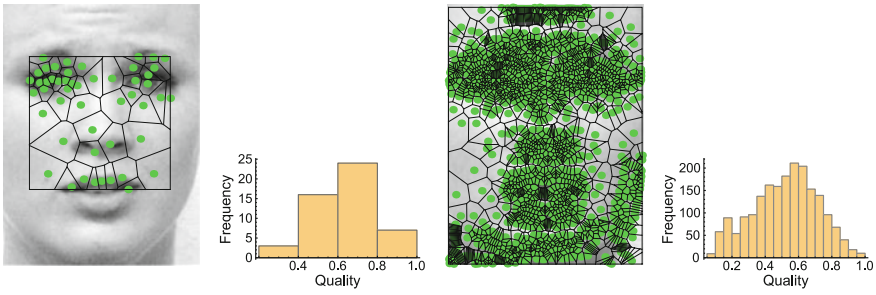

2.19.1: ⌜Centroids 2.19.2: ⌜Cent. Histogram 2.19.3: $\overline{\wedge}$Centroids 2.19.4: $\overline{\wedge}$Cent. Histogram

Fig. 2.19 Corner and edge centroid tessellations and quality histograms [39, Sect. 6]

centroid-corners are distributed in the image. The tessellation of the face in Fig. 2.19.1 is generated by sites that are image ⌐Centroids that are also corner pixels and the tessellation of the face in Fig. 2.19.3 is generated by sites that are image $\overline{\wedge}$Centroids that are also edge pixels. The poor quality of the $\overline{\wedge}$Centroids-based tessellation can be seen in the unevenness of the site quality distribution in Fig. 2.19.4. From this, it is apparent that the greater the number of high quality tessellation cells, the higher the quality of the image tessellation. ■

Conjecture 2.45 *A high quality digital image tessellation reflects the fact that high quality cells are more prevalent in the tessellated image.* ■

In practical terms, for the tessellation of a digital image, if each pair of sites is connected by a straight edge for an image $img1$, the resulting shape more readily approximates a corresponding shape derived from the edge-connected sites from an image $img2$ representing a class of images. Let $s_1, \ldots, s_n \in S$, a set of n sites. For each image, the edge-connected site form a path from s_1 to s_n.

The set of sites S is **connected**, provided, for all $p, q \in S$, there is a sequence $p_0, \ldots, p_m$ of sites in S so that $p = p_0$ and $q = p_n$ and site p_i is closest to site p_{i-1} for $1 \leq i \leq m$. The sequence $p_0, \ldots, p_m$ is called a **path**. What we want is a pathwise-connected set of sites. The set S is **pathwise-connected**, provided, for every pair of sites in X, there is a path connecting the sites. Pathwise-connected sites yield a **connected-sites shape** (denoted by ⚽).

Let f be a continuous mapping of a set of sites $S1$ for a test image to the Euclidean plane $\mathbb{R}^2$. Further, let $f(S1)$ be the ⚽ shape of the pathwise-connected sites on test image $img1$. Similarly, let g be a continuous mapping of a set of sites $S2$ for a test image to the Euclidean plane $\mathbb{R}^2$. In addition, let $g(S2)$ be the ⚽ shape of the pathwise-connected sites on $img2$ that represents a class of shapes. If the ⚽ shape $f(S1)$ is similar in structure to the ⚽ shape of $g(S2)$, then $f(S1)$ can deformed (mapped) to $f(S2)$. This means that all of the points in $f(S1)$ map to $f(S2)$. If ⚽ shape $f(S1)$ deforms into ⚽ shape $g(S2)$, then ⚽ shape $f(S1)$ belongs to the $g(S2)$ shapes class and $img1$ belongs to the $img2$ class of images.

The approximation of ⚽ shape $g(S2)$ with ⚽ shape $f(S1)$ enters into this, by computing the distance $D(f(S1), g(S2))$ defined by

$$D(f(S1), g(S2)) = inf\{\|f(x) - g(y)\| : x \in S_1, y \in S_2\}.$$

Let $\varepsilon > 0$ be a small real number. The ⚽ shape of $g(S2)$ is a good approximation of the ⚽ shape of $f(S1)$, provided $D(f(S1), g(S2)) < \varepsilon$. In that case, ⚽ shape $f(S1)$ approximates the members in the $g(S2)$ shapes class. The more closely shape $f(S1)$ approximates shape $g(S2)$, the higher the likelihood that $img1$ belongs to the $img2$ class of images. For more about the comparison of shapes, see Sect. 5.1.

Remark 2.46 **Image Quality and Geometric Reconstruction**.
Image geometry and the structure of objects embedded in an image are revealed by careful selection of mesh generating points, leading to an image cover with a high

quality mesh. A digital image often is a very complex object with its own inherent geometry, which is difficult to detect. The basic computational proximity approach in solving the image geometry detection problem is to

1^o Reconstruct the geometry of an image, approximating what escapes the eye. This can be done using an approach such as the one introduced by A. Vacavant, D. Cocurjolly, and L. Tougne [44]. See, also, A. Kuba, L.G. Nyúl and K. Palágyi [45] on image geometry.

2^o Tessellate part or all of an image with convex shapes.

3^o Inspect the structural similaries of the sets of convex shapes in an image tessellation.

4^o Carry out image quality assessment using a measure such as the structural similarity index measure (SSIM) introduced by Z. Wang, A.C. Bovik, H.R. Sheikh, and E.P. Simoncelli [46]:

$$SSIM(x, y) = \frac{(2\mu_x\mu_y + C_1)(2\sigma_{xy} + C_2)}{(\mu_x^2 + \mu_y^2 + C_1)(\sigma_x^2 + \sigma_y^2 + C_2)}.$$

The SSIM measures the statistical characteristics of signals x, y in the terms the mean value, variances, cross correlation between the standard deviations and constants C_1 and C_2. ■

Problem 2.47 Do the following:

1^o Select a digital image img.

2^o Select a set of sites (generating points) S.

3^o 🚲 Tessellate the image img with a Voronoï diagram $V(S)$.

4^o Compute the SSIM(S) for the sets of sites S, using values of C_1 and C_2 of your own choosing.

5^o Let q_i be the quality of each polygon in the diagram $V(S)$ using Field's approach. Then, for N polygons in $V(S)$, compute q_{all} from [39]:

$$q_{all} = \frac{1}{N}\sum_{i=1}^{N} q_i$$

6^o ☕ Compare the SSIM value with the q_{all} value.

7^o Repeat the above steps for 10 different images and construct a table showing the comparison between the SSIM(S) and q_{all} values. What can you conclude for the values in your comparison? ■

Remark 2.48 **Line Detection and Fragmentation Quality**.
Another approach to measuring the quality of a tessellation and, indirectly, the quality of a digital image is to consider the fragmentation quality measure[4] introduced by L. Wenyin and D. Dori [47]. The CP approach in applying the Wenyin-Dori line segment fragmentation quality measure is summarized in the following steps.

[4]Many thanks to A. Vacavant for pointing this out.

1^o Select a digital image img.
2^o Select a set of sites (generating points) S.
3^o Tessellate the image img with a Voronoï diagram $V(S)$.
4^o Tessellate the image img with a Delaunay triangulation $De(S)$. Notice the edges of the Delaunay triangles and the Voronoï region polygons overlap. It is this overlap of each pair of line segments (one from a Delaunay triangle and the other from a Voronoï polygon) that provides a basis for the next step.
5^o Compute the quality of overlappingline segments using $Q_b(k)$ (formula (23) in [47]). ■

Problem 2.49 Do the following:
1^o Select a digital image img.
2^o Select a set of sites (generating points) S.
3^o 🚲 Tessellate the image img with a Voronoï diagram $V(S)$.
4^o 🚲 Tessellate the image img with a Delaunay triangulation $De(S)$.
5^o Compute the SSIM(S) for the sets of sites S, using values of C_1 and C_2 of your own choosing.
6^o Let q_i be the quality of each polygon in the diagram $V(S)$ using Field's approach. Then, for N polygons in $V(S)$, compute

$$q_{all} = \frac{1}{N}\sum_{i=1}^{N} q_i$$

7^o Compute the line fragmentation measure $Q_b(k)$ from Remark 2.48. Do this for each of pair of line segments from the overlapping line segments in diagram $V(S)$ and triangulation $De(S)$.
8^o ☕ Compare the SSIM value with the q_{all} and $Q_b(k)$ values.
9^o Repeat the above steps for 10 different images and construct a table showing the comparison between the SSIM(S), q_{all} and $Q_b(k)$ values. What can you conclude for the values in your comparison? ■

2.10 Tessellation Region Centroids

A *Voronoï tessellation* of a plane surface X is a collection of closed planar regions derived from a set of sites S (generating points). Let $s \in S$ be one of the sites. A Voronoï region V_s consists of all points in X that are closer to s than to any other site in S. Let $\rho : X \to (R)$ be a density function on X, $x \in X$. A *centroid* is a center of mass s^* of a region V. It corresponds to a measure of central location for a region, defined by

$$s^* = \frac{\int_V x\rho(x)dx}{\int_V \rho(x)dx}.$$

For more details about region centroids, see [35, p. 638]. Using Mathematica, generate Voronoï regions from a given set of sites.

Using Mathematica script 3 on a set of random numbers used as region sites, we generate the Voronoï regions shown in Fig. 2.20.

Mscript 3 Generating Voronoï Regions.

(*Find centroids in a Dirichlet tessellation using RegionCentroid.*)

***pts* = *RandomReal*[1, {100, 2}];**

$\mathcal{R}$ = *VoronoiMesh*[*pts*, {{0, 1}, {0, 1}}] ■

Next, using MScript 28 in Appendix A.2 on regions in a Voronoï tessellation, determine the region centroids shown in Fig. 2.21.

Example 2.50 **Sample Region Centroids**.
Sample collections of Voronoï regions in Fig. 2.20 are generated using Mathematica10 Mscript 3 using as sites random numbers. These sites are shown as a collection of black dots in Fig. 2.21. Next, Mscript 2 is used to find the centroid of each Voronoï region (see Fig. 2.21). ■

2.11 Centroid-Based Voronoï Mesh on an Image

This section introduces the construction of centroid-based Voronoï meshes on digital images. Voronoï regions are a source of centroids used as a source of sites in the generate a Voronoï mesh $\mathscr{M}$. The steps in the construction of centroid-based Voronoï mesh are given in Algorithm 3.

Example 2.51 **Centroidal Voronoï Mesh Scripts**.
Algorithm 3 is implemented in two different ways in Appendix A.2. Matlab Listing A.1 in Appendix A.2 finds image segment centroids, which are used to construct a Voronoï mesh on an image. MScript 29 uses a different approach in implementing Algorithm 3. First, image corners are used to construct a Voronoï mesh (each Voronoï region is an image segment). Then the centroids in each corner-based Voronoï region are found. Those region centroids are a source of sites used to construct a centroid-based Voronoï mesh. ■

Example 2.52 **Centroidal Voronoï Mesh on an Image**.
MScript 29 in Appendix A.2 is used on a camera image to find a set centroids that serve as sites in constructing a Voronoï mesh (shown in Fig. 2.22.1). The locations of centroids in the Voronoï regions are shown with ● bullets in Fig. 2.22.2. The centroids on a Nikon® camera image are shown in Fig. 2.23.1 and centroidal Voronoï mesh superimposed on the camera image is shown in Fig. 2.23.2. Putting these results to together leads to the Voronoï mesh plus region centroids superimposed on the camera image in Fig. 2.24. ■

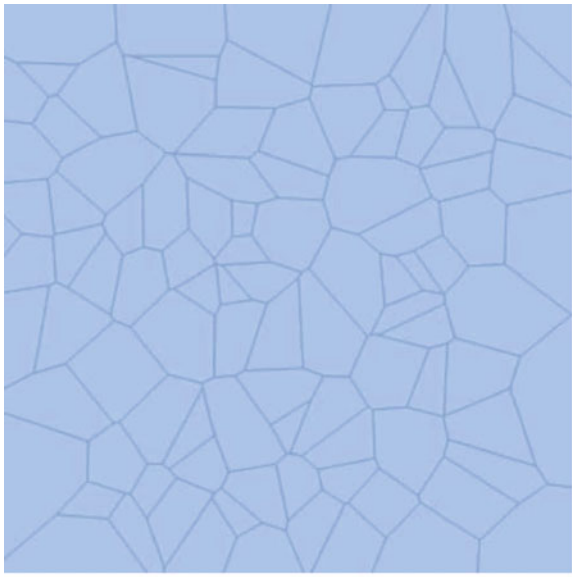

2.20.1: Centroid-Based Tessellation

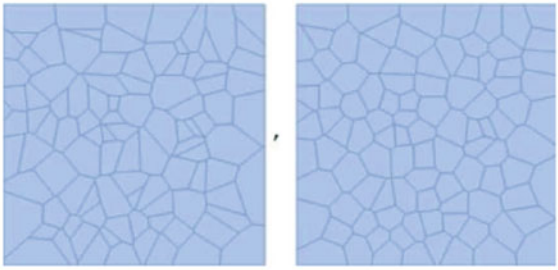

2.20.2: Tessellation Regions1

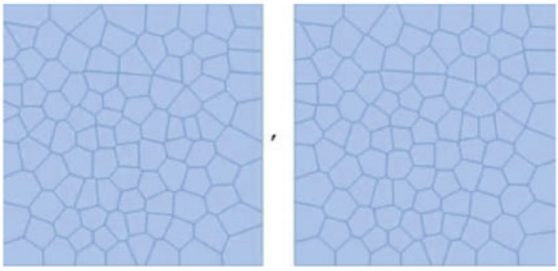

2.20.3: Tessellation Regions2

Fig. 2.20 Sample tessellation derived from randomly selected sites

Problem 2.53 Use Mathematica to construct a centroid-based Voronoï mesh on 3 digital images of your choosing. In solving this problem, do the following:

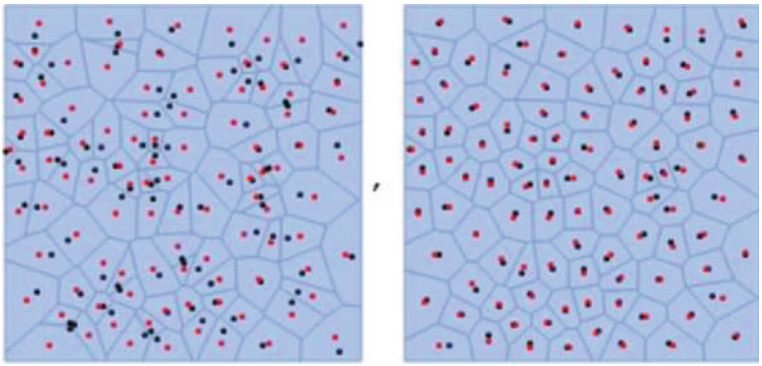

2.21.1: Centroids1

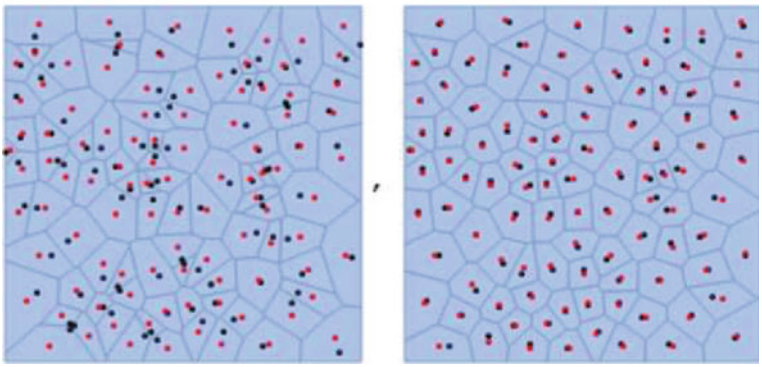

2.21.2: Centroids2

Fig. 2.21 Region centroids detected

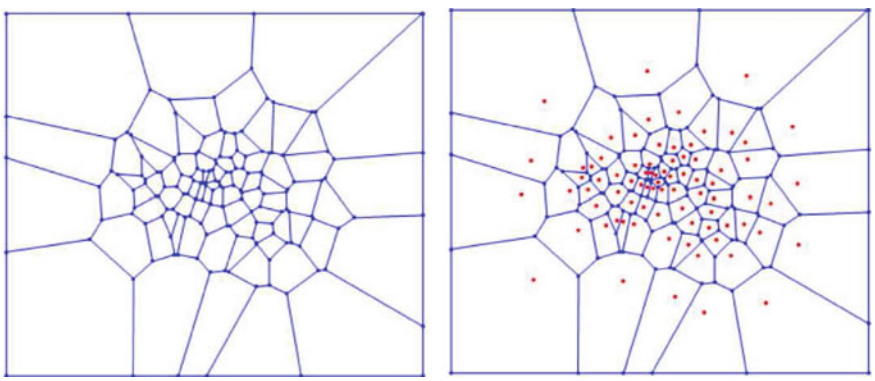

2.22.1: Voronoï Mesh 2.22.2: Centroids on Mesh

Fig. 2.22 Centroidal Voronoï mesh

2.23.1: Centroids on Mesh

2.23.2: Voronoï Mesh

Fig. 2.23 Centroidal Voronoï mesh on image

Fig. 2.24 Centroidal Voronoï mesh on a Nikon® camera image

1^o Segment each image using the watershed method. **Hint**: See Sect. 9.11 on watershed segmentation.
2^o Find the centroid of watershed segment.
3^o Following steps 3 to 7 in Algorithm 3, superimpose a centroidal mesh on each image. ■

Problem 2.54 Use Mathematica to implement Step 8 in Algorithm 3 to find several mesh nerves in 3 digital images of your choosing. In each case, the mesh nerves are embedded in a centroidal Voronoï mesh. Highlight the Voronoï regions in each mesh nerve with an appropriate colour, using the opacity property on the parts of the underlying regions are visible after colouring the regions. ■

Algorithm 3: Construct Centroidal Voronoï Mesh on a Digital Image

Input : Read digital image img.
Output: Centroid-based Voronoï mesh $\mathscr{M}$

```
1 img ⟼ segmentedImg;
2 segmentedImg ⟼ segmentCentroids;
3 S ← segmentCentroidsCoordinates;
4 /* S contains segment centroid coordinates used as mesh generating points
  (sites). */ ;
5 S ⟼ img ;
6 S ⟼ VoronoiMesh ℳ;
7 VoronoiMesh ℳ ⟼ img ;
8 /* Use Algorithm 1 to construct image mesh nerves in ℳ. */ ;
```

Problem 2.55 Use Mathematica to implement Step 8 in Algorithm 3 to find several mesh nerves so that the centers of mesh nerves are $\overset{\emptyset}{\Subset}$-strongly far from each other in 3 digital images of your choosing. In each case, the mesh nerves are embedded in a centroidal Voronoï mesh. Highlight the Voronoï regions in each mesh nerve center with an appropriate colour, using the opacity property so that the parts of the underlying regions are visible after colouring the regions. ■

Problem 2.56 Use Mathematica to implement Step 8 in Algorithm 3 to find several mesh nerves so that the centers of mesh nerves are $\overset{\wedge\wedge}{\delta}_{\Phi}$-strongly far *descriptively* from each other in 3 digital images of your choosing. In each case, the mesh nerves are embedded in a centroidal Voronoï mesh. Highlight the Voronoï regions in each mesh nerve center with an appropriate colour, using the opacity property so that the parts of the underlying regions are visible after colouring the regions. ■

Problem 2.57 ☕ Give three examples of centers of mesh nerves that are $\overset{\emptyset}{\Subset}$-strongly far from each other and $\overset{\wedge\wedge}{\delta}_{\Phi}$-strongly near each other *descriptively*. This means that strongly far centers of mesh nerves have a nonempty descriptive intersection. Let X a nonempty collection of image mesh nerves, $(X, \left\{\overset{\emptyset}{\Subset}, \overset{\wedge\wedge}{\delta}_{\Phi}\right\})$ a proximity space endowed with the $\overset{\emptyset}{\Subset}$ and $\overset{\wedge\wedge}{\delta}_{\Phi}$ proximities, and let $A, B \subset X$ be a pair of image mesh nerves. We know that $A \overset{\emptyset}{\Subset} B$ is possible from the examples already given. Now give examples so that

$$A \overset{\emptyset}{\Subset} B \text{ and } A \underset{\Phi}{\cap} B \neq \emptyset. \quad \blacksquare$$

Problem 2.58 Use Mathematica to implement Step 8 in Algorithm 3 to find several mesh nerves so that the mesh nerves are $\overset{\wedge\wedge}{\delta}$-strongly near each other in 3 digital images

of your choosing. In each case, the mesh nerves are embedded in a centroidal Voronoï mesh. Highlight the adjacent Voronoï regions in the strongly near mesh nerves with an appropriate colour, using the opacity property so that the parts of the underlying regions are visible after colouring the regions. **Hint**: Voronoï mesh nerves A and B are $\overset{\wedge\wedge}{\delta}$-strongly near, provided A has a Voronoï region edge in common with B. ■

Conjecture 2.59 *The centers of $\overset{\wedge\wedge}{\delta}$-strongly near image mesh nerves are $\overset{\not\delta}{\vee}$-strongly far from each other.* ■

Problem 2.60 Prove Conjecture 2.59. ■

Conjecture 2.61 *The centers of all image mesh nerves are $\overset{\not\delta}{\vee}$-strongly far from each other.* ■

Problem 2.62 Prove Conjecture 2.61. ■

References

1. Beer, G., Di Concilio, A., Di Maio, G., Naimpally, S., Pareek, C., Peters, J.: Somashekhar Naimpally, 1931–2014. Topol. Appl. **188**, 97–109 (2015). doi:10.1016/j.topol.2015.03.010, MR3339114
2. Naimpally, S., Warrack, B.: Proximity Spaces. Cambridge Tract in Mathematics, vol. 59. Cambridge University Press, Cambridge (1970). X + 128 pp., Paperback (2008)
3. Riesz, F.: Stetigkeitsbegriff und abstrakte mengenlehre. Atti del IV Congresso Internazionale dei Matematici, vol. II, pp. 182–109 (1908)
4. Naimpally, S.: Near and far. A centennial tribute to Frigyes Riesz. Siberian Electronic Mathematical Reports, vol. 2, pp. 144–153 (2009)
5. Naimpally, S.: Proximity Approach to Problems in Topology and Analysis. Oldenbourg Verlag, Munich (2009). 73 pp., ISBN 978-3-486-58917-7, MR2526304
6. Di Concilio, A.: Proximal set-open topologies on partial maps. Acta Math. Hung. **88**(3), 227–237 (2000). MR1767801
7. Di Concilio, A.: Topologizing homeomorphism groups of rim-compact spaces. Topol. Appl. **153**(11), 1867–1885 (2006)
8. Di Concilio, A.: Proximity: a powerful tool in extension theory, functions spaces, hyperspaces, boolean algebras and point-free geometry. In: Mynard, F., Pearl, E. (eds.) Beyond Topology, AMS Contemporary Mathematics, vol. 486, pp. 89–114. American Mathematical Society, Providence (2009)
9. Čech, E.: Topological Spaces. Wiley, London (1966). Fr seminar, Brno, 1936–1939; rev. ed. Z. Frolik, M. Katětov
10. Efremovič, V.: The geometry of proximity I (in Russian). Mat. Sb. (N.S.) 31(73)(1), 189–200 (1952)
11. Naimpally, S.: Proximity Spaces. Cambridge University Press, Cambridge (1970). X + 128 pp., ISBN 978-0-521-09183-1
12. Peters, J., Ramanna, S.: Pattern discovery with local near sets. In: Alarcón, R., Barceló, P. (eds.) Proceedings of the Jornadas Chilenas de Computación 2012 Workshop on Pattern Recognition, pp. 1–4. The Chilean Computing Society, Valparaiso (2012)
13. Peters, J., Naimpally, S.: Applications of near sets. Notices Am. Math. Soc. **59**(4), 536–542 (2012). http://dx.doi.org/10.1090/noti817, MR2951956

14. Naimpally, S., Peters, J.: Topology with applications. Topological spaces via near and far. World Scientific, Singapore (2013). Xv + 277 pp. Am. Math. Soc. MR3075111
15. Di Maio, G., Naimpally, S.A., Meccariello, E.: Theory and applications of proximity, nearness and uniformity. Seconda Università di Napoli, Napoli (2009), 264pp., MR1269778
16. Naimpally, S., Peters, J., Wolski, M.: Foreword [near set theory and applications]. Math. Comput. Sci. **7**(1), 1–2 (2013)
17. Peters, J.: Topology of digital images - visual pattern discovery in proximity spaces, intelligent systems reference library, vol. 63. Springer, Berlin (2014). Xv + 411 pp. Zentralblatt MATH Zbl 1295 68010
18. Kuratowski, C.: Topologie I. Panstwowe Wydawnictwo Naukowe, Warsaw (1958). XIII + 494 pp
19. Guadagni, C.: Bornological convergences on local proximity spaces and ω_μ-metric spaces. Ph.D. thesis, Università degli Studi di Salerno, Salerno (2015). Supervisor: A. Di Concilio, 79 pp
20. Ronse, C.: Regular open or closed sets. Philips Research Laboratory Series, Brussels WD59, pp. 1–8 (1990)
21. Wallman, H.: Lattices and topological spaces. Ann. Math. **39**(1), 112–126 (1938)
22. Lodato, M.: On topologically induced generalized proximity relations. Ph.D. thesis. Rutgers University (1962). Supervisor: S. Leader
23. Lodato, M.: On topologically induced generalized proximity relations I. Proc. Am. Math. Soc. **15**, 417–422 (1964)
24. Lodato, M.: On topologically induced generalized proximity relations II. Pac. J. Math. **17**, 131–135 (1966)
25. Delaunay, B.D.: Sur la sphère vide. Izvestia Akad. Nauk SSSR, Otdelenie Matematicheskii i Estestvennyka Nauk **7**, 793–800 (1934)
26. Edelsbrunner, H.: A Short Course in Computational Geometry and Topology. Springer, Berlin (2014). 110 pp
27. Peters, J.: Proximal Voronoï regions, convex polygons, and leader uniform topology. Adv. Math.: Sci. J. **4**(1), 1–5 (2015)
28. Edelsbrunner, H.: Geometry and Topology of Mesh Generation. Cambridge University Press, Cambridge (2001). 209 pp
29. Peters, J.: Proximal Delaunay triangulation regions, pp. 1–4 (2014). arXiv:1411.6260
30. Voronoï, G.: Sur un problème du calcul des fonctions asymptotiques. J. für die reine und angewandte Math. **126**, 241–282 (1903)
31. Voronoï, G.: Nouvelles applications des paramètres continus à la théorie des formes quadratiques. J. für die reine und angewandte Math. **133**, 97–178 (1907). JFM 38.0261.01
32. Voronoï, G.: Nouvelles applications des paramètres continus à la théorie des formes quadratiques. J. für die reine und angewandte Math. **134**, 198–287 (1908). JFM 39.0274.01
33. Frank, N., Hart, S.: A dynamical system using the Voronoi tessellation. Am. Math. Monthly **117**(2), 92–112 (2010)
34. Dirichlet, G.: Über die reduktion der positiven quadratischen formen mit drei unbestimmten ganzen zahlen. J. für die reine und angewandte **40**, 221–239 (1850). MR
35. Du, Q., Faber, V., Gunzburger, M.: Centroidal voronoi tessellations: applications and algorithms. SIAM Rev. **41**(4), 637–676 (1999). MR
36. Weisstein, E.: Voronoi diagram. Wolfram MathWorld (2014). http://mathworld.wolfram.com/VoronoiDiagram.html
37. Willard, S.: General Topology. Dover Publications Inc, Mineola (1970). Xii + 369 pp, ISBN: 0-486-43479-6 54-02, MR0264581
38. Leader, S.: On clusters in proximity spaces. Fundamenta Mathematicae **47**, 205–213 (1959)
39. A-iyeh, E., Peters, J.: Measure of tessellation quality of voronoï meshes. Theory Appl. Math. Comput. Sci. **5**(2), 158–185 (2015)
40. Shewchuk, J.: What is a good linear element? interpolation, conditioning, and quality measures. Technical report, University of California at Berkeley (2015). http://www.cs.berkeley.edu/jrs/papers/elem.pdf

41. Bhatia, R., Lawrence, K.: Two-dimensional finite element mesh generation based on stripwise automatic triangulation. Comput. Struct. **36**(2), 309–319 (1990)
42. Bank, R., Xu, J.: An algorithm for coarsening unstructured meshes. Numer. Math. **73**, 1–36 (1996)
43. Field, D.: Qualitative measures for initial meshes. Int. J. Numer. Methods Eng. **47**, 887–906 (2000)
44. Vacavant, A., Cocurjolly, D., Tougne, L.: Topological and geometrical reconstruction of complex objects on irregular isothetic grids. In: Kuba, A., Nyúl, L., Palágyi, K. (eds.) Discrete Geometry for Computer Imagery. Lecture Notes in Computer Science, vol. 4245, pp. 470–481. Springer, Heidelberg (2006)
45. Kuba, A., Nyúl, L., Palágyi, K.: Discrete Geometry for Computer Imagery. Lecture Notes in Computer Science, vol. 4245. Springer, Berlin (2006). Xiv + 688 pp. ISBN: 3-540-47651-2, MR2307269
46. Wang, Z., Bovik, A., Sheikh, H., Simoncelli, E.: Image quality assessment: from error visibility to structural similarity. IEEE Trans. Image Process. **13**(4), 600–612 (2004)
47. Wenyin, L., Dori, D.: A protocol for performance evaluation for line detection algorithms. Mach. Vis. Appl. **9**, 240–250 (1997)

http://www.springer.com/978-3-319-30260-7

Computational Proximity
Excursions in the Topology of Digital Images
Peters, J.F.
2016, XXVIII, 433 p. 254 illus., 39 illus. in color.,
Hardcover
ISBN: 978-3-319-30260-7